

Optical Engineering

OpticalEngineering.SPIEDigitalLibrary.org

2.5- and 5-Gbps time-delay self-homodyne interference differential phase-shift keying optical receiver for space-to-ground communication link

Yanan Zhi
Jianfeng Sun
Yu Zhou
Wei Lu
Enwen Dai
Weiqing Pan
Liren Liu

2.5- and 5-Gbps time-delay self-homodyne interference differential phase-shift keying optical receiver for space-to-ground communication link

Yanan Zhi,^{a,*} Jianfeng Sun,^b Yu Zhou,^b Wei Lu,^b Enwen Dai,^b Weiqing Pan,^a and Liren Liu^b

^aZhejiang University of Science and Technology, Laboratory of 3-D Optics and Depth Sensing Technology, Zhejiang, China

^bChinese Academy of Sciences, Shanghai Institute of Optics and Fine Mechanics, Key Laboratory of Space Laser Communication and Detection Technology, Shanghai, China

Abstract. The availability and reliability of the high data rate space-to-ground optical coherent communication links are critically challenged because the wave front of the signal beam is distorted and impaired when propagating through atmospheric turbulence. Based on the free-space interference of two successive data bits delayed by an unequal-arm-length Mach–Zehnder interferometer (MZI), a pupil-matching time-delay self-homodyne interference differential phase-shift keying (DPSK) optical receiver with 2×4 90-deg optical hybrid is designed for the high data rate space-to-ground optical communication links due to its immunity from wave front impairment. The delayed optical path difference (OPD) in the unequal-arm-length MZI corresponds to the duration of one bit and can be stabilized to below 1000th of the wavelength by the closed-loop feedback control. The maximum system insertion loss is <1 dB. The measurement accuracy of OPD in unequal-arm-length MZI is 0.01 mm by the deramping method from a chirped laser. The double-bit-rate 2.5-/5-Gbps DPSK optical receiver has been presented. Parallel and separate atmospheric measurement along the optical communication link is also performed simultaneously. The 2.5- and 5-Gbps optical communication links have already been verified with a $\phi 300$ -mm receiving telescope between two buildings in downtown over a distance of 2.4 km in the worst-case atmospheric conditions. The measured bit-error-rate is better than 10^{-6} . Without wave front compensation of the adaptive optics, local oscillator, and optical phase-locked loops, the pupil-matching time-delay self-homodyne interference DPSK optical receiver has great significance for future developments of space-to-ground optical communication links. © The Authors. Published by SPIE under a Creative Commons Attribution 4.0 Unported License. Distribution or reproduction of this work in whole or in part requires full attribution of the original publication, including its DOI. [DOI: [10.1117/1.OE.58.1.016114](https://doi.org/10.1117/1.OE.58.1.016114)]

Keywords: self-homodyne interference; differential phase-shift keying, optical receiver; 2×4 90-deg optical hybrid; space-to-ground communication link; unequal-arm-length Mach–Zehnder interferometer.

Paper 181283 received Sep. 5, 2018; accepted for publication Jan. 3, 2019; published online Jan. 28, 2019.

1 Introduction

Free-space optical communications, including remote optical communications between deep space, geosynchronous orbit (GEO), medium earth orbit, low earth orbit (LEO) satellites, high-altitude platform, airborne platform, and optical ground station (OGS), can compose an integrated space-ground real-time high-speed optical communication network in the future.¹ With a larger communication capacity, larger aperture gains, and smaller diffraction losses at optical wavelengths as compared to radio frequency (RF) wavelengths, free-space optical communications can offer many potential benefits for future space missions by enabling higher data rate links with reduced size, weight, and power burden on a spacecraft and smaller ground terminals on the Earth, and break through the bottleneck of RF communication. In 2001, the European Space Agency (ESA) successfully performed semi-conductor inter satellite link experiment, the world's first intersatellite 50-Mbps laser communication link experiment based on incoherent intensity-modulated/direct-detection modulation between GEO and LEO satellites.² Since that time, a series of duplex optical link experiments between GEO/LEO satellites and OGS have been verified.^{3–9} The homodyne binary phase-shift-keying

(BPSK) systems can achieve the best receiver sensitivity and the longest transmission distance among all optical communication systems.¹⁰ In 2008, an optical intersatellite communication link based on the homodyne BPSK transmitted data with a bidirectional data rate of 5.625 Gbps with a bit-error-rate (BER) better than 10^{-9} between two LEO satellites.^{11,12} The first demonstration of a BPSK laser communication link from LEO to OGS at 5.625 Gbps was reported in 2010.^{13,14} These results demonstrate the applicability of free-space optical communication for not only high data rate intersatellite optical links, but also space-to-ground optical links. However, BPSK free-space optical communication is critically challenged by the effects of atmospheric turbulence in practical deployment. The refractive index inhomogeneity generated by atmospheric turbulence distorts the phase integrity of the propagating beam (shown in Fig. 1), which is vital for high data rate BPSK demodulation. The link performance will be seriously degraded because the interference contrast is deteriorated when a signal beam is mixed with a local oscillator (LO) laser.¹⁵

Atmospheric turbulence has been well-studied and well-described using the Kolmogorov theory by Fried.¹⁶ Several techniques have been performed to mitigate the effects of atmospheric turbulence to increase the heterodyne efficiency and signal to noise ratio (SNR) of space-to-ground optical communication links. Small apertures can be adopted

*Address all correspondence to Yanan Zhi, E-mail: zhiyanan@zust.edu.cn

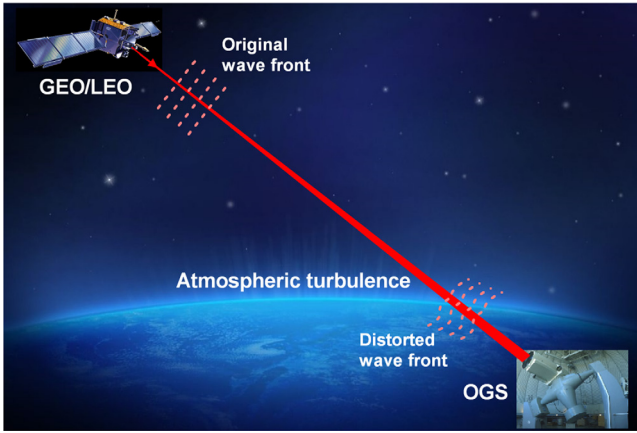


Fig. 1 The sketch map of atmospheric turbulence distorting the wave front of the propagating beam in the space-to-ground coherent communication downlink. GEO, geosynchronous orbit satellite; LEO, low-earth orbit satellite; and OGS, optical ground station.

when the wave front deformations are small within a certain diameter if the aperture is smaller than the Fried parameter. In 2011, the ESA demonstrated 5.625-Gbps bidirectional laser communication between an LEO [near-field infrared experiment (NFIRE)] and a ground communication terminal with a 65-mm diameter aperture of TESAT OGS hosted in Tenerife.¹³ However, using small apertures results in low received power and strong intensity fluctuations. The adaptive optics (AO) can measure the deformations of a received wave front using a Shack–Hartmann sensor and finish the corresponding corrections by applying inverse deformations with a deformable mirror. The AO schemes to mitigate the atmospheric turbulence have been investigated for satellite-to-ground laser communication in ESA OGS.^{17,18} The mixing efficiency and the BER performances of the closed-loop AO integrated with the coherent optical communications were analyzed.^{19–21} Different AO approaches for OGS were presented and compared.²² Although the AO was proven to be a very promising technique that can largely improve the performances of the space-to-ground optical communication links, the complex systems and expensive costs limit its application. The orbital angular momentum (OAM) has the potential for enabling multiplexing of multiple data-carrying beams to increase the transmission capacity and spectral efficiency of a communication system. A phase correction method for OAM states was proposed to mitigate the turbulent aberrations more effectively.²³ The low-density parity-check coded OAM modulation scheme was proved to be suitable for the high data rate free-space optical communication link under strong atmospheric turbulence.²⁴ Increasing the spacing between the detected OAM modes was also shown to effectively mitigate the effects of atmospheric turbulence.²⁵ A hybrid input–output–algorithm-based AO system has been proposed to compensate the distorted OAM-based free-space optical communication systems.²⁶ However, the complexity and high cost of the schemes also limit their applications in the implementation of space-to-ground optical communication links.

Time-delay self-homodyne interference differential phase-shift keying (DPSK) is a promising alternative to AO and OAM for overcoming atmospheric turbulence. Time-delay self-homodyne interference DPSK is based on the interference of two successive data bits in an unequal-

arm-length interferometer, where the delayed optical path difference (OPD) corresponds to the duration of one bit. The relative phases of two successive data bits can be converted into the intensity by the interference. The modulation contrast in an interferometer depends on the interference of successive wave fronts, not on the quality of the wave front itself. So, without wave front compensation of AO, time-delay self-homodyne interference DPSK can completely eliminate wave front distortions if the two interfering bits experience identical distortions when passing the atmospheric turbulence. A 5.625-Gbps multimode Michelson-type DPSK interferometer was developed for the satellite-to-ground communication in the ESA's OGS.²⁷ The unequal-arm-length MZI-based coherent DPSK receiver has also been proposed.^{28,29} In this paper, the 2.5- and 5-Gbps pupil-matching time-delayed self-homodyne interference DPSK optical receivers based on the free-space unequal-arm-length MZI and 2×4 90-deg optical hybrid³⁰ for space-to-ground optical communication link are designed and verified between two buildings in the downtown area over a distance of 2.4 km in the worst-case atmospheric conditions.

2 Theoretical Analysis

2.1 Time-Delay Self-Homodyne Interference DPSK Receiver

DPSK modulation has already been successfully applied in high data rate optical fiber communications and has recently gained significant research attention.³¹ Using differential decoding in the BPSK transmitter, bit 1 will be transmitted by a shift the phase of the modulated signal π relative to the previous phase of the modulated signal. Bit 0 will be transmitted without a shift of the phase of the modulated signal relative to the previous modulated signal. The encoding operation is described mathematically by

$$S'_n(t) = S_n(t) \oplus S'_{n-1}(t - \tau_B), \quad (1)$$

where $S_n(t)$ is the baseband signal, $S'_n(t)$ is the DPSK signal, and $S'_{n-1}(t - \tau_B)$ is the adjacent DPSK signal at a time interval of τ_B . τ_B is the duration of one bit. The \oplus denotes the Boolean XOR operator.

DPSK modulation for free-space optical communication through an atmospheric channel is based on the interference of two successive data bits in an unequal-arm-length interferometer (depicted by Fig. 2). It is the time-delay self-homodyne interference without independent LO and optical phase-locked loop (OPLL). The relations between the baseband signal $S(t)$, DPSK signal $S'(t)$, DPSK phase signal $\varphi(t)$, delayed DPSK phase signal $\varphi(t - \tau_d)$, phase of the self-homodyne interference $\varphi(t) - \varphi(t - \tau_d)$, and recovered signal $S_r(t)$ are shown in Fig. 3. The one-to-one match between the baseband signal and received interference pattern should be underlined. The delayed time τ_d and the corresponding delayed OPD in air ΔL_{OPD} can be determined by

$$\begin{cases} \tau_d = \tau_B = \frac{1}{B}, \\ \Delta L_{\text{OPD}} = \frac{c}{B}, \end{cases} \quad (2)$$

where B is the transmission bandwidth and c is the velocity of light. The delayed OPD corresponds to the duration of one bit: at a data rate of 2.5 Gbps, the duration of one bit is 0.4 ns,

the homodyne BPSK. Because the unequal-arm-length interferometer superimposes the identical wave fronts, the optimum modulation contrast is obtained despite a distorted input wave front. This is the physical basis of time-delay self-homodyne interference DPSK systems. In this way, the time-delay self-homodyne interference DPSK receiver can be immune from wave front distortion when passing through the atmospheric turbulence and is suited for high data rate space-to-ground coherent optical communication links. In this paper, the free-space unequal-arm-length MZI is used as the time-delay self-homodyne interference DPSK optical receiver.

2.2 Free-Space Unequal-Arm-Length MZI-DPSK Receiver with 2 × 4 90-deg Optical Hybrid

The schematic diagram of an unequal-arm-length MZI-DPSK receiver with 2 × 4 90-deg optical hybrid is presented in Fig. 4. The Jones' polarization matrix calculus is employed to describe the light wave field. The input signal with the unknown polarization can be given by

$$\vec{E}_S = E_S \begin{bmatrix} k_1 \\ k_2 \end{bmatrix} \exp\{i[\varphi(t) + \psi_N(t)]\}, \quad (3)$$

where E_S is the amplitude of the light wave. k_1 and k_2 are the components of the x and y coordinates, respectively. $\varphi(t)$ is the modulated phase function of the signal beam. $\psi_N(t)$ is the noise phase caused by atmospheric turbulence and is the difficult problem to be resolved in this research. Note that the time factor of the light wave has been ignored.

The matrix of half-waveplate HWP1 is $\Lambda_{\text{HWP1}} = \begin{bmatrix} \cos 2\alpha_1 & \sin 2\alpha_1 \\ \sin 2\alpha_1 & -\cos 2\alpha_1 \end{bmatrix}$, where α_1 is the angle of the principal axes tilted to the x coordinate. Thus the passed field \vec{E}'_S is given by

$$\begin{cases} \vec{E}'_S = \Lambda_{\text{HWP1}} \vec{E}_S = E_S \begin{bmatrix} \eta \\ \kappa \end{bmatrix} \exp\{i[\varphi(t) + \psi_N(t)]\} \\ \eta = k_1 \cos 2\alpha_1 + k_2 \sin 2\alpha_1 \\ \kappa = k_1 \sin 2\alpha_1 - k_2 \cos 2\alpha_1 \end{cases}, \quad (4)$$

where η and κ are the component of the x and y coordinates, respectively. PBS1 and PBS2 act as the splitter and combiner in the unequal-arm-length MZI, respectively. PBS1 is considered to be a nonideal polarization beam splitter. The reflection and transmission matrix of PBS1 are given by

$$\Lambda_{\text{PBS1}} = \begin{cases} R_1 = \begin{bmatrix} 0 & 0 \\ 0 & r_{v-1} \exp(i\rho_{v-1}) \end{bmatrix} \\ T_1 = \begin{bmatrix} t_{p-1} \exp(it\tau_{p-1}) & 0 \\ 0 & 0 \end{bmatrix} \end{cases},$$

$$\begin{cases} \vec{E}''_{S,1} = \Lambda_{\text{HWP2}} \vec{E}'_{S,1} = \frac{\sqrt{2}}{2} \begin{bmatrix} 1 \\ 1 \end{bmatrix} \eta t_{p-1} E_S \exp\{i[\varphi(t) + \tau_{p-1} + \psi_N(t)]\} \\ \vec{E}''_{S,2} = \Lambda_{\text{QWP}} \vec{E}'_{S,2} = \frac{\sqrt{2}}{2} \begin{cases} \exp\left[i\left(\frac{\pi}{4} + 2\varepsilon\right)\right] \\ \exp\left(-i\frac{\pi}{4}\right) \end{cases} \kappa r_{v-1} E_S \exp\{i[\varphi(t - \tau_d) + \rho_{v-1} + \psi_N(t - \tau_d)] + \sigma(t)\} \end{cases}. \quad (6)$$

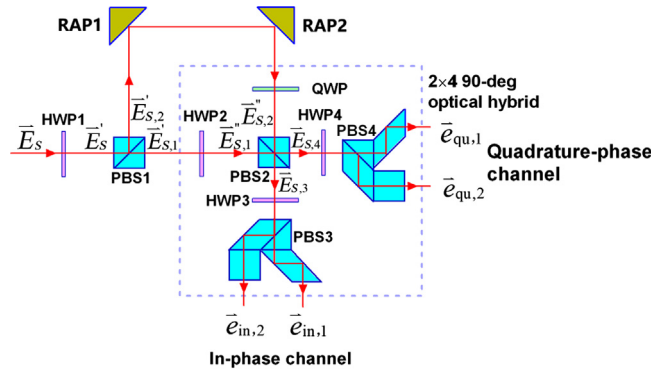


Fig. 4 The schematic diagram of free-space unequal-arm-length MZI-DPSK receiver with 2 × 4 90-deg optical hybrid. Polarization beam splitter (PBS), polarization beam splitter; HWP, half-waveplate; QWP, quarter-waveplate; RAP, right angle prism. The 2 × 4 90-deg optical hybrid is indicated by the blue dashed box.

where ρ_{v-1} is the phase shift of the reflection matrix; τ_{p-1} is the induced phase shift of the transmission matrix; r_{v-1} is the amplitude of the reflection matrix; t_{p-1} is the amplitude of the transmission matrix. After passing the splitter PBS1, the two divided beams in the unequal-arm-length MZI can be given by

$$\begin{cases} \vec{E}'_{S,1} = T_1 \vec{E}_S = t_{p-1} \eta E_S \begin{bmatrix} 1 \\ 0 \end{bmatrix} \exp\{i[\varphi(t) + \tau_{p-1} + \psi_N(t)]\} \\ \vec{E}'_{S,2} = R_1 \vec{E}_S = r_{v-1} \kappa E_S \begin{bmatrix} 0 \\ 1 \end{bmatrix} \exp\{i[\varphi(t) + \rho_{v-1} + \psi_N(t)]\} \end{cases}. \quad (5)$$

After entering the following 2 × 4 90-deg optical hybrid, the beam $\vec{E}'_{S,1}$ passes the half-waveplate (HWP2) and the beam $\vec{E}'_{S,2}$ passes the quarter-waveplate (QWP) before reaching the combiner PBS2.

Assuming that the half-waveplate HWP2 has a principal axis tilted by $\frac{\pi}{8}$ to the x coordinate, the matrix can be given by

$$\Lambda_{\text{HWP2}} = \frac{\sqrt{2}}{2} \begin{bmatrix} 1 & 1 \\ 1 & -1 \end{bmatrix}.$$

Assuming that the QWP has a principal axis tilted by $\frac{\pi}{4} + \varepsilon$ to the x coordinate, the matrix can be given by

$$\Lambda_{\text{QWP}} = \frac{1}{2}(1 + i) \begin{bmatrix} 1 + i \sin 2\varepsilon & -i \cos 2\varepsilon \\ -i \cos 2\varepsilon & 1 - i \sin 2\varepsilon \end{bmatrix},$$

where $\varepsilon \ll \frac{\pi}{2}$ and the small angle approximation can be performed. Taking the delay time τ_d and the random noise phase $\sigma(t)$ between the two optical paths into consideration, the passed fields before the combiner PBS2 can be presented as

PBS2 is also considered to be a nonideal polarization beam splitter. The reflection and transmission matrices of PBS2 are given by

$$\Lambda_{\text{PBS2}} = \begin{cases} R_2 = \begin{bmatrix} 0 & 0 \\ 0 & r_{v,2} \exp(i\rho_{v,2}) \end{bmatrix} \\ T_2 = \begin{bmatrix} t_{p,2} \exp(i\tau_{p,2}) & 0 \\ 0 & 0 \end{bmatrix} \end{cases}.$$

After passing the combiner PBS2, the divided two beams can be given by

$$\begin{cases} \vec{E}_{S,3} = R_2 \vec{E}_{S,1}'' + T_2 \vec{E}_{S,2}'' = \frac{\sqrt{2}}{2} E_S \begin{pmatrix} t_{p,2} r_{v,1} \kappa \exp\{i[\varphi(t - \tau_d) + \rho_{v,1} + \tau_{p,2} + \psi_N(t - \tau_d) + \sigma(t) + 2\varepsilon - \frac{\pi}{4}]\} \\ t_{p,1} r_{v,2} \eta \exp\{i[\varphi(t) + \tau_{p,1} + \rho_{v,2} + \psi_N(t)]\} \end{pmatrix} \\ \vec{E}_{S,4} = T_2 \vec{E}_{S,1}'' + R_2 \vec{E}_{S,2}'' = \frac{\sqrt{2}}{2} E_S \begin{pmatrix} t_{p,1} t_{p,2} \eta \exp\{i[\varphi(t) + \tau_{p,1} + \tau_{p,2} + \psi_N(t)]\} \\ r_{v,1} r_{v,2} \kappa \exp\{i[\varphi(t - \tau_d) + \rho_{v,1} + \rho_{v,2} + \psi_N(t - \tau_d) + \sigma(t) + \frac{\pi}{4}]\} \end{pmatrix} \end{cases}. \quad (7)$$

Assuming that the half-waveplates HWP3 and HWP4 have the principal axes tilted by α_3 and α_4 to the x coordinate, respectively then the matrix can be given by

$$\Lambda_{\text{HWP3}} = \begin{bmatrix} \cos 2\alpha_3 & \sin 2\alpha_3 \\ \sin 2\alpha_3 & -\cos 2\alpha_3 \end{bmatrix},$$

$$\Lambda_{\text{HWP4}} = \begin{bmatrix} \cos 2\alpha_4 & \sin 2\alpha_4 \\ \sin 2\alpha_4 & -\cos 2\alpha_4 \end{bmatrix},$$

where both PBS3 and PBS4 are considered to be nonideal polarization beam splitters. The matrices of PBS3 and PBS4 are given by

$$\Lambda_{\text{PBS3}} = \begin{cases} R_3 = \begin{bmatrix} 0 & 0 \\ 0 & r_{v,3} \exp(i\rho_{v,3}) \end{bmatrix} \\ T_3 = \begin{bmatrix} t_{p,3} \exp(i\tau_{p,3}) & 0 \\ 0 & 0 \end{bmatrix} \end{cases},$$

$$\Lambda_{\text{PBS4}} = \begin{cases} R_4 = \begin{bmatrix} 0 & 0 \\ 0 & r_{v,4} \exp(i\rho_{v,4}) \end{bmatrix} \\ T_4 = \begin{bmatrix} t_{p,4} \exp(i\tau_{p,4}) & 0 \\ 0 & 0 \end{bmatrix} \end{cases}.$$

The four output fields are given by

$$\begin{cases} \vec{e}_{\text{in},1} = T_3 \Lambda_{\text{HWP3}} \vec{E}_{S,3} \\ \vec{e}_{\text{in},2} = R_3 \Lambda_{\text{HWP3}} \vec{E}_{S,3} \\ \vec{e}_{\text{qu},1} = T_4 \Lambda_{\text{HWP4}} \vec{E}_{S,4} \\ \vec{e}_{\text{qu},2} = R_4 \Lambda_{\text{HWP4}} \vec{E}_{S,4} \end{cases}. \quad (8)$$

Thus, the four electrical signal outputs can be given by

$$\begin{cases} I_{\text{in},1} = |\vec{e}_{\text{in},1}|^2 = I_{\text{dc},\text{in},1} + \frac{1}{2} r_{v,1} t_{p,1} r_{v,2} t_{p,2} t_{p,3}^2 \kappa \eta \sin 4\alpha_3 E_S^2 k_{\text{in}} \\ \quad \times \cos \left[\varphi(t) - \varphi(t - \tau_d) + \psi_N(t) - \psi_N(t - \tau_d) + (\tau_{p,1} + \rho_{v,2} - \rho_{v,1} - \tau_{p,2}) - 2\varepsilon - \sigma(t) + \frac{\pi}{4} \right] \\ I_{\text{in},2} = |\vec{e}_{\text{in},2}|^2 = I_{\text{dc},\text{in},2} + \frac{1}{2} r_{v,1} t_{p,1} r_{v,2} t_{p,2} t_{v,3}^2 \kappa \eta \sin 4\alpha_3 E_S^2 k_{\text{in}} \\ \quad \times \cos \left[\varphi(t) - \varphi(t - \tau_d) + \psi_N(t) - \psi_N(t - \tau_d) + (\tau_{p,1} + \rho_{v,2} - \rho_{v,1} - \tau_{p,2}) - 2\varepsilon - \sigma(t) + \frac{\pi}{4} + \pi \right] \\ I_{\text{qu},1} = |\vec{e}_{\text{qu},1}|^2 = I_{\text{dc},\text{qu},1} + \frac{1}{2} r_{v,1} t_{p,1} r_{v,2} t_{p,2} t_{p,4}^2 \kappa \eta \sin 4\alpha_4 E_S^2 k_{\text{qu}} \\ \quad \times \cos \left[\varphi(t) - \varphi(t - \tau_d) + \psi_N(t) - \psi_N(t - \tau_d) + (\tau_{p,1} + \tau_{p,2} - \rho_{v,1} - \rho_{v,2}) - \sigma(t) - \frac{\pi}{4} \right] \\ I_{\text{qu},2} = |\vec{e}_{\text{qu},2}|^2 = I_{\text{dc},\text{qu},2} + \frac{1}{2} r_{v,1} t_{p,1} r_{v,2} t_{p,2} t_{v,4}^2 \kappa \eta \sin 4\alpha_4 E_S^2 k_{\text{qu}} \\ \quad \times \cos \left[\varphi(t) - \varphi(t - \tau_d) + \psi_N(t) - \psi_N(t - \tau_d) + (\tau_{p,1} + \tau_{p,2} - \rho_{v,1} - \rho_{v,2}) - \sigma(t) - \frac{\pi}{4} + \pi \right] \end{cases}. \quad (9)$$

The corresponding DC coefficients can be presented as

$$\begin{cases} I_{dc_in,1} = \frac{1}{2}[r_{v-1}t_{p-2}t_{p-3}\kappa \cos 2\alpha_3 E_S]^2 k_{in} + \frac{1}{2}[t_{p-1}r_{v-2}t_{p-3}\eta \sin 2\alpha_3 E_S]^2 k_{in} \\ I_{dc_in,2} = \frac{1}{2}[r_{v-1}t_{p-2}r_{v-3}\kappa \sin 2\alpha_3 E_S]^2 k_{in} + \frac{1}{2}[t_{p-1}r_{v-2}r_{v-3}\eta \cos 2\alpha_3 E_S]^2 k_{in} \\ I_{dc_qu,1} = \frac{1}{2}[t_{p-1}t_{p-2}t_{p-4}\eta \cos 2\alpha_4 E_S]^2 k_{qu} + \frac{1}{2}[r_{v-1}r_{v-2}t_{p-4}\kappa \sin 2\alpha_4 E_S]^2 k_{qu} \\ I_{dc_qu,2} = \frac{1}{2}[t_{p-1}t_{p-2}r_{v-4}\eta \sin 2\alpha_4 E_S]^2 k_{qu} + \frac{1}{2}[r_{v-1}r_{v-2}r_{v-4}\kappa \cos 2\alpha_4 E_S]^2 k_{qu} \end{cases} \quad (10)$$

where k_{in} and k_{qu} are the photodetector responsivities of the in-phase and quadrature-phase channels, respectively. Two pairs of 180-deg phase-shifted outputs are obtained: one pair ($I_{in,1}$ and $I_{in,2}$) is the in-phase branch, and the other pair ($I_{qu,1}$ and $I_{qu,2}$) is the quadrature-phase branch.

In order to realize balanced detection, the DC components must be eliminated. The tilted α_3 and α_4 of HWP3 and HWP4 can be satisfied by

$$\begin{cases} (\tan 2\alpha_3)^2 = \frac{(r_{v-1}t_{p-2}t_{p-3})^2 \kappa^2 - (t_{p-1}r_{v-2}r_{v-3})^2 \eta^2}{(r_{v-1}t_{p-2}r_{v-3})^2 \kappa^2 - (t_{p-1}r_{v-2}t_{p-3})^2 \eta^2} \\ (\tan 2\alpha_4)^2 = \frac{(r_{v-1}r_{v-2}r_{v-4})^2 \kappa^2 - (t_{p-1}t_{p-2}t_{p-4})^2 \eta^2}{(r_{v-1}r_{v-2}t_{p-4})^2 \kappa^2 - (t_{p-1}t_{p-2}r_{v-4})^2 \eta^2} \end{cases} \quad (11)$$

The in-phase and quadrature-phase output can be given by

$$\begin{cases} I_{in} = I_{in,1} - I_{in,2} = \frac{1}{2}r_{v-1}t_{p-1}r_{v-2}t_{p-2}\kappa\eta \sin 4\alpha_3 k_{in} E_S^2 \\ \cos \left[\varphi(t) - \varphi(t - \tau_d) + \psi_N(t) - \psi_N(t - \tau_d) + (\tau_{p-1} - \rho_{v-1}) - (\tau_{p-2} - \rho_{v-2}) - 2\varepsilon - \sigma(t) + \frac{\pi}{4} \right] \\ I_{qu} = I_{qu,1} - I_{qu,2} = \frac{1}{2}r_{v-1}t_{p-1}r_{v-2}t_{p-2}\kappa\eta \sin 4\alpha_4 k_{qu} E_S^2 \\ \cos \left[\varphi(t) - \varphi(t - \tau_d) + \psi_N(t) - \psi_N(t - \tau_d) + (\tau_{p-1} - \rho_{v-1}) + (\tau_{p-2} - \rho_{v-2}) - \sigma(t) - \frac{\pi}{4} \right] \end{cases} \quad (12)$$

If the small angle ε can be satisfied by

$$\varepsilon = \rho_{v-2} - \tau_{p-2}. \quad (13)$$

The residual phase difference induced by PBS2 can be removed. So, rotating the quarter waveplate QWP by a small angle ε , the accurate phase difference $\frac{\pi}{4}$ between the in-phase and quadrature channels can be guaranteed despite the polarization behavior of beam combiner PBS2.

The noise phase $\psi_N(t)$ caused by atmospheric turbulence is considered to be slow varying compared with the high-

speed data rate. So $\psi_N(t)$ can be removed in the unequal-arm-length MZI-DPSK receiver by

$$\psi_N(t) - \psi_N(t - \tau_d) = 0. \quad (14)$$

The mathematical derivation manifests the feasibility to eliminate the noise phase caused by atmospheric turbulence by use of the unequal-arm-length MZI-DPSK receiver.

For the high-speed balanced detectors, the in-phase channel and quadrature-phase channel photocurrents are given by

$$\begin{cases} I_{in} = I_{in,1} - I_{in,2} = \frac{1}{2}r_{v-1}t_{p-1}r_{v-2}t_{p-2}\kappa\eta \sin 4\alpha_3 k_{in} E_S^2 \cos[\varphi(t) - \varphi(t - \tau_d) - \sigma(t)] \\ I_{qu} = I_{qu,1} - I_{qu,2} = \frac{1}{2}r_{v-1}t_{p-1}r_{v-2}t_{p-2}\kappa\eta \sin 4\alpha_4 k_{qu} E_S^2 \sin[\varphi(t) - \varphi(t - \tau_d) - \sigma(t)] \end{cases} \quad (15)$$

The phase can be extracted by multiplying both the in-phase and quadrature-phase signals. Finally, the high-speed phase signal $\varphi(t) - \varphi(t - \tau_d)$ can be extracted from the obtained phase after being high-pass filtered. The low-speed random phase noise $\sigma(t)$ produced between the two optical paths in the unequal-arm-length can be extracted from the obtained phase after being low-pass filtered. The closed-loop feedback control can be realized by compensating the low-speed random phase noise in order to stabilize the OPD and eventually optimize the receiver performance.

3 Design and Experimental Verification

3.1 Design of High Data Rate Optical Communication Link

The block diagram of the high data rate space-to-ground optical communication link based on a free-space unequal-arm-length MZI-DPSK receiver is shown in Fig. 5. The optical communication link includes the transmitting module, receiving module, and atmospheric channel. The transmitting module is composed of a 1550-nm laser source, digital

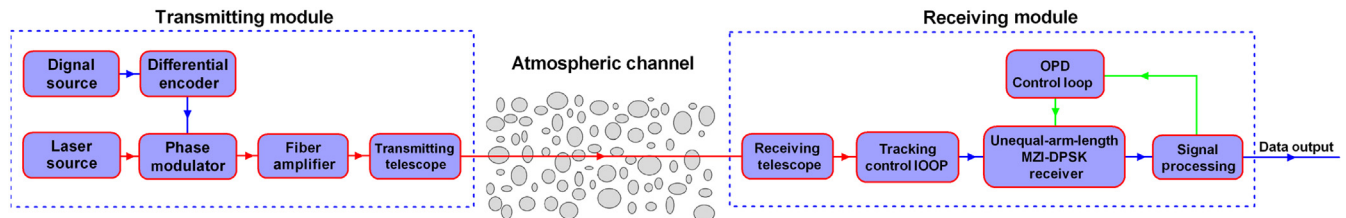


Fig. 5 The block diagram of high data-rate optical communication link based on free-space unequal-arm-length MZI-DPSK receiver including transmitting module and receiving modules.

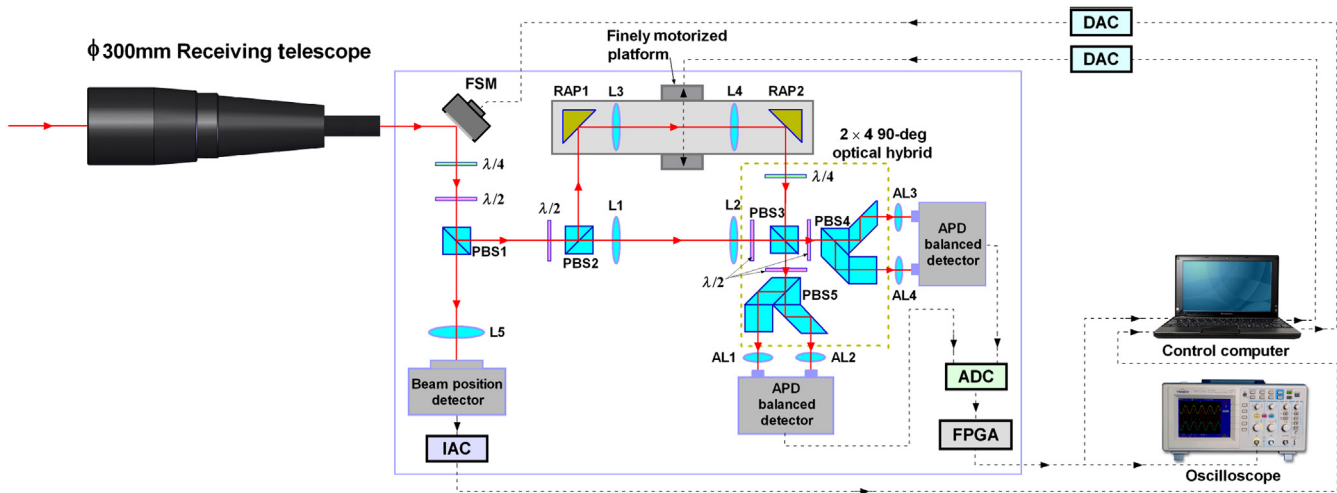


Fig. 6 The schematic of the receiving module based on unequal-arm-length MZI-DPSK receiver. PBS, polarization beam splitter; $\lambda/2$, half-waveplate; $\lambda/4$, quarter-waveplate; FSM, fast steering mirror; L, lens; AL, aspheric lens; RAP, right-angle prism (protected gold coating); FPGA, field-programmable gate array; ADC, analog to digital converter; DAC, digital-to-analog converter; and IAC, image acquisition card.

source, differential encoder, high-speed phase modulator, erbium-doped fiber amplifier, and transmitting telescope. Taking the high-speed relative motion between the satellite and the ground terminal into consideration, only the circularly polarized light can be fit for the future satellite-ground optical communication link. So the circularly polarized light is used and transmitted from the $\phi 50$ -mm transmitting telescope in this work. The nonreturn-to-zero DPSK method is used for laser beam modulation, and the bit rate is up to 2.5 and 5 Gbps, respectively. The receiving module is composed of a receiving telescope, tracking control loop for intensity stabilization, unequal-arm-length MZI-DPSK receiver, OPD control loop for OPD stabilization, and a signal processing unit. The near-diffraction-limited beam is propagated from the transmitting telescope to a $\phi 300$ -mm receiving telescope over an atmospheric channel with a distance of 2.4 km between two buildings in downtown.

3.2 Design of Receiving Module Based on Free-Space Unequal-Arm-Length MZI-DPSK

Figure 6 depicts the schematic of the receiving module based on a free-space unequal-arm-length MZI-DPSK. The circularly polarized input beam light from the receiving telescope is collimated, and the tip/tilt correction is performed at the internal pupil using a fast steering mirror (FSM). After being reflected by the FSM, the circularly polarized beam passes a QWP, which converts it into linearly polarized light. The linearly polarized signal beam can be adjusted by the HWP in front of PBS1. PBS1 acts as a splitter for beam position detection and unequal-arm-length MZI-DPSK. The beam position detection is performed by Xenics infrared CCD camera. The infrared CCD camera, FSM, image acquisition card (IAC), digital-to-analog converter (DAC), and control computer compose the tracking control module in order to inhibit the influence of beam wandering,³² angle-of-arrival fluctuation, and scintillation.³³ The double 4-f confocal lens groups (L1–L4) work as the pupil matching in order to eliminate the wave front aberration resulting from the diffraction in the unequal-arm-length MZI for optimized

coherent detection.³⁴ The maximum system insertion loss is measured to be <1 dB.

The self-developed 10-GHz bandwidth avalanche photodiode balanced detectors with double aspheric lenses are used for the high-speed balanced photodetection. The field-programmable gate array (FPGA) is used for high-speed data acquisition, phase demodulation, and corresponding filtering. The random phase noise is extracted, and the feedback control signal is generated for the finely motorized platform, which works as an OPD compensation. The high-dynamics, very stable piezo-nano-positioner is applied as the finely motorized platform to optimize and stabilize the OPD. The positioning resolution is 0.05 nm and the pitch is ± 5 μ rad. The high-response bandwidth of the hardware is up to 10 kHz. In this work, the OPD can be stabilized to below one thousandth of the wavelength.

Figure 7 shows the 3D design of a free-space unequal-arm-length MZI-DPSK receiver for a 5-Gbps optical

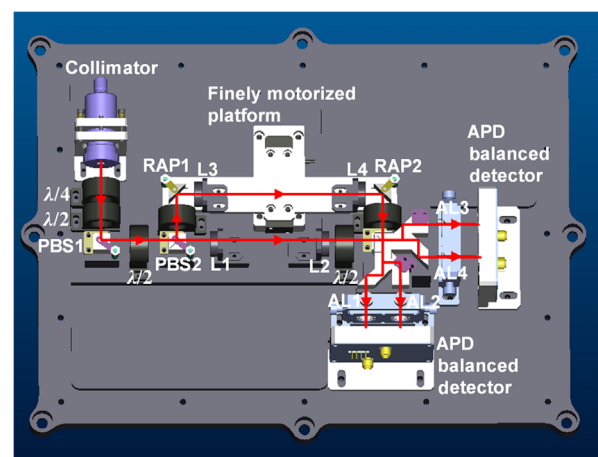


Fig. 7 The 3-D design schematic of unequal-arm-length MZI-DPSK receiver for 5-Gbps optical communication link. PBS, polarization beam splitter; $\lambda/2$, half-waveplate; $\lambda/4$, quarter-waveplate; L, lens; AL, aspheric lens; and RAP, right-angle prism.

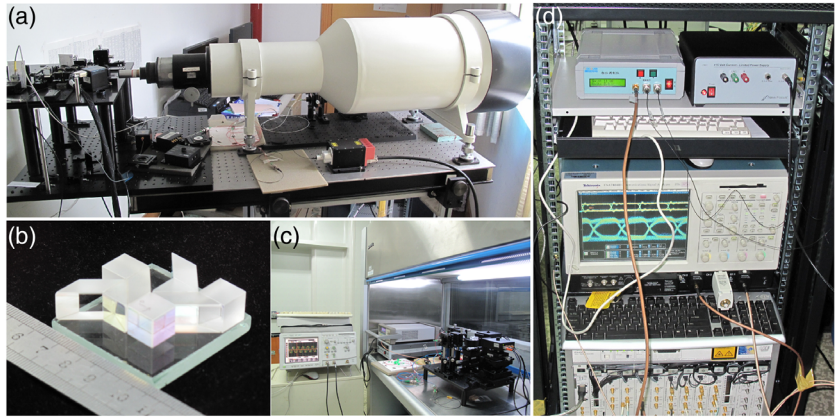


Fig. 8 (a) The picture of the high data-rate free-space optical communication link based on unequal-arm-length MZI-DPSK receiver, (b) the picture of free-space 2×4 90-deg optical hybrid with compact structure, (c) the picture of orthogonal receiving module including the free-space 2×4 90-deg optical hybrid and the balanced photodetectors, and (d) the picture of the working electronic equipments during the indoor link testing.

communication link. Note that the input collimator is just for system debugging and will be removed during the link experiment. Figure 8(a) shows the picture of the high data-rate free-space optical communication link based on free-space unequal-arm-length MZI-DPSK receiver. Figure 8(b) shows the picture of a free-space 2×4 90-deg optical hybrid with a compact structure. Figure 8(c) shows the picture of an orthogonal receiving module including the free-space 2×4 90-deg optical hybrid and the balanced photodetectors. Figure 8(d) shows the working electronic equipment, including the BER Tester, digital oscilloscope, electro-optic phase modulator, and power supply, during the indoor link testing.

3.3 OPD Measurement in Free-Space Unequal-Arm-Length MZI

The data rate of 2.5 Gbps is equivalent to an OPD of 120 mm in air, and the data rate of 5 Gbps is equivalent to an OPD of

60 mm in air. From Eq. (2), the error of the bit rate can be determined by

$$\frac{dB}{d(\Delta L_{OPD})} = -\frac{c}{(\Delta L_{OPD})^2}, \quad (16)$$

where B is the transmission bandwidth, c is the velocity of light, and ΔL_{OPD} is the delayed OPD in air. Thus, the measurement accuracy of OPD in a free-space unequal-arm-length MZI is very critical for a high data-rate optical communication link. However, accurate OPD measurement in unequal-arm-length MZI is difficult to achieve by the general geometry method. Here, a scheme based on the deramping method from a chirped laser is presented and shown in Fig. 9. The chirped frequency for the OPD measurement can be given by

$$f(t) = f_0 + \frac{1}{2}\dot{f}t, \quad (17)$$

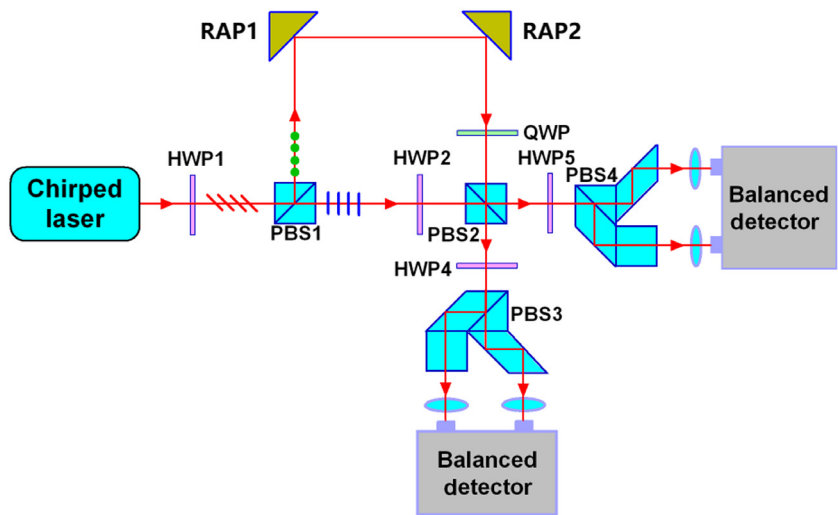


Fig. 9 The schematic of the accurate OPD measurement in free-space unequal-arm-length MZI based on deramping method from a chirped laser. PBS, polarization beam splitter; HWP, half-waveplates; QWP, quarter-waveplates; and RAP, right angle prism.

where f_0 is the initial frequency and \bar{f} is the chirp rate of the frequency.

The generated beat frequency F_b can be given by

$$F_b = \bar{f}\tau_d = \bar{f} \frac{\Delta L_{\text{OPD}}}{c} = -\frac{\bar{\lambda}}{\lambda^2} \Delta L_{\text{OPD}}, \quad (18)$$

where $\bar{\lambda}$ is the chirp rate of the wavelength. So, the OPD in an unequal-arm-length MZI can be calculated by measuring the beat frequency. In this work, the chirp light source is a Newfocus TLB-6800 single-mode tunable laser, and the chirp rate of the wavelength is 250 nm/s. The spectral resolution of the spectrum analyzer is 1 nm. In this way, the measurement accuracy of the OPD in an unequal-arm-length MZI is 0.01 mm.

3.4 Double-bit-rate 2.5/5-Gbps Free-Space Unequal-Arm-Length MZI-DPSK Optical Receiver

Because of the one-to-one correspondence between the bit rate and OPD, the bit rate of the optical communication link can only be determined by the OPD in an unequal-arm-length MZI. In order to realize the variable bit rate optical communication link between LEO/GEO satellite and OGS, a double-bit-rate 2.5/5-Gbps free-space unequal-arm-length MZI-DPSK optical receiver is proposed in Fig. 10. The unequal-arm-length MZI for 2.5 Gbps is composed of PBS2, PBS3, PBS8, PBS9, L1, L2, L5, and L6. The unequal-arm-length MZI for 5 Gbps is composed of PBS2, PBS3, PBS6, PBS7, L1, L2, L3, and L4. By the gate actions of the HWP

and PBS, the 2.5- and 5-Gbps bit rates can be adopted, respectively. The minimum crosstalk between the two channels is larger than 30 dB.

3.5 Atmospheric Measurement

The parallel and separate atmospheric measurement along the optical communication link is also performed simultaneously by the scintillometer between two buildings in downtown over a distance of 2.4 km. The typical 24-h (from 7:30 am, breeze, clear weather) atmospheric measurement results including Fried coherence parameter r_0 and turbulence structure profile C_n^2 are shown in Figs. 11(a) and 11(b). Figures 11(c) and 11(d) show the pictures of the transmitter (TX) and receiver (RX) modules of the Scintec scintillometer, respectively. From Fig. 10(a) and 10(b), as the representatives of atmospheric turbulence, the nonlinear variations of r_0 and C_n^2 have an approximately inverse relation. In the morning, the atmospheric turbulence changes violently because of the combined action of sunshine and wind. The typical r_0 is within 10 mm, and the typical C_n^2 is larger than $5 \times 10^{-13} \text{ m}^{-2/3}$. In this strong turbulent environment, the typical C_n^2 is even larger than $10^{-12} \text{ m}^{-2/3}$. In the afternoon, the atmospheric turbulence tends to weaken as the temperature decreases. The r_0 varies from about 10 to 30 mm, and the C_n^2 varies from 10^{-13} to $10^{-14} \text{ m}^{-2/3}$ in this relatively moderate turbulent environment. In the night, the typical r_0 varies from about 20 to 40 mm, and the typical C_n^2 is $10^{-14} \text{ m}^{-2/3}$ in this relatively weak turbulent environment. Most of our optical communication link

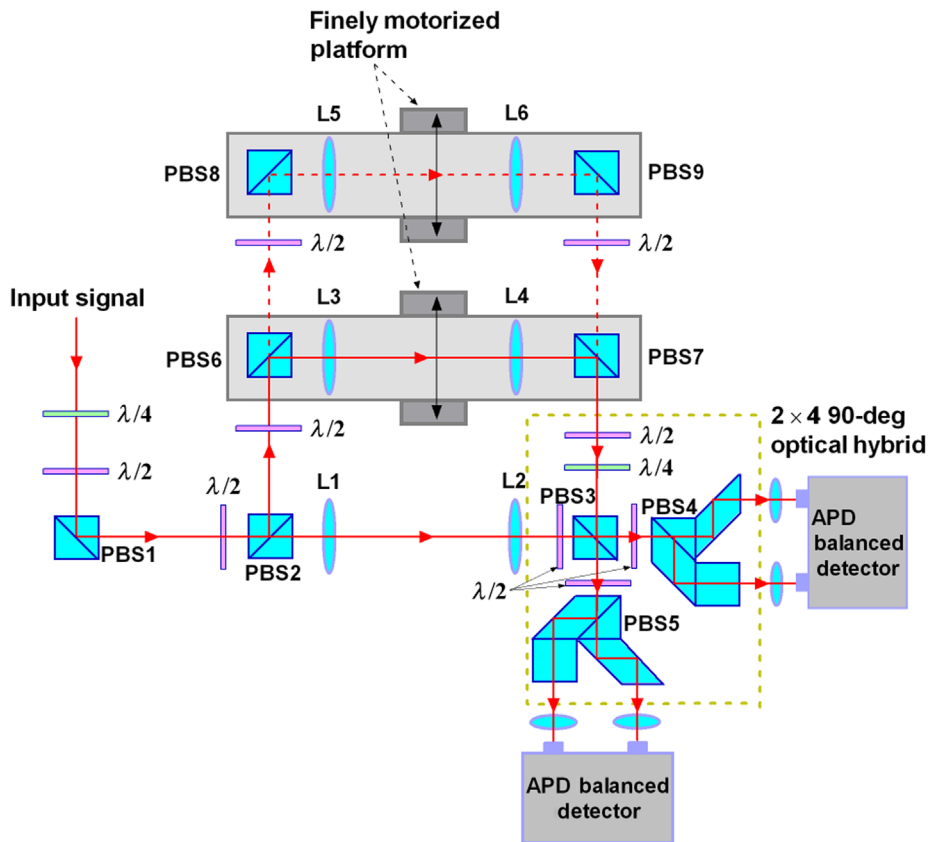


Fig. 10 The schematic of the double-bit-rate 2.5/5-Gbps free-space unequal-arm-length MZI-DPSK optical receiver. PBS, polarization beam splitter; $\lambda/2$, half-waveplate; $\lambda/4$, quarter-waveplate; and L, lens. The 2×4 90-deg optical hybrid is indicated by the yellow dashed box.

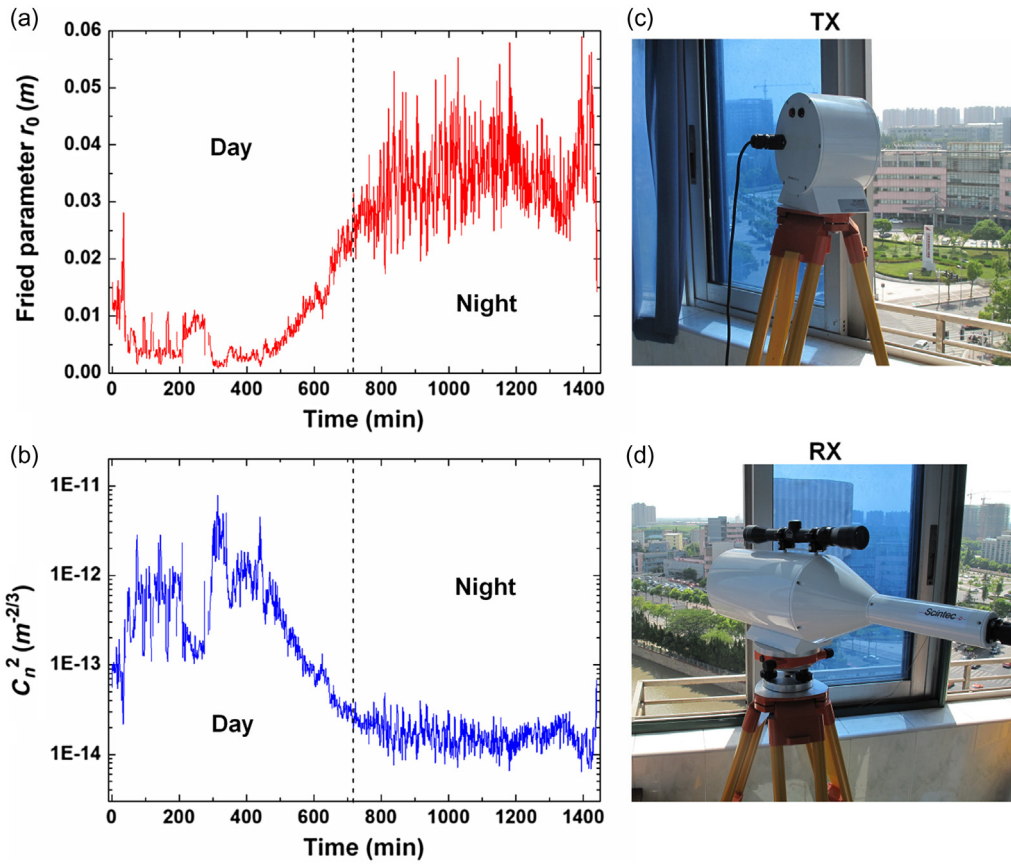


Fig. 11 The typical results and picture of atmospheric measurement: (a) Fried coherence parameter r_0 , (b) turbulence structure profile C_n^2 , (c) TX module of the Scintec scintillometer, and (d) RX module of the Scintec scintillometer.

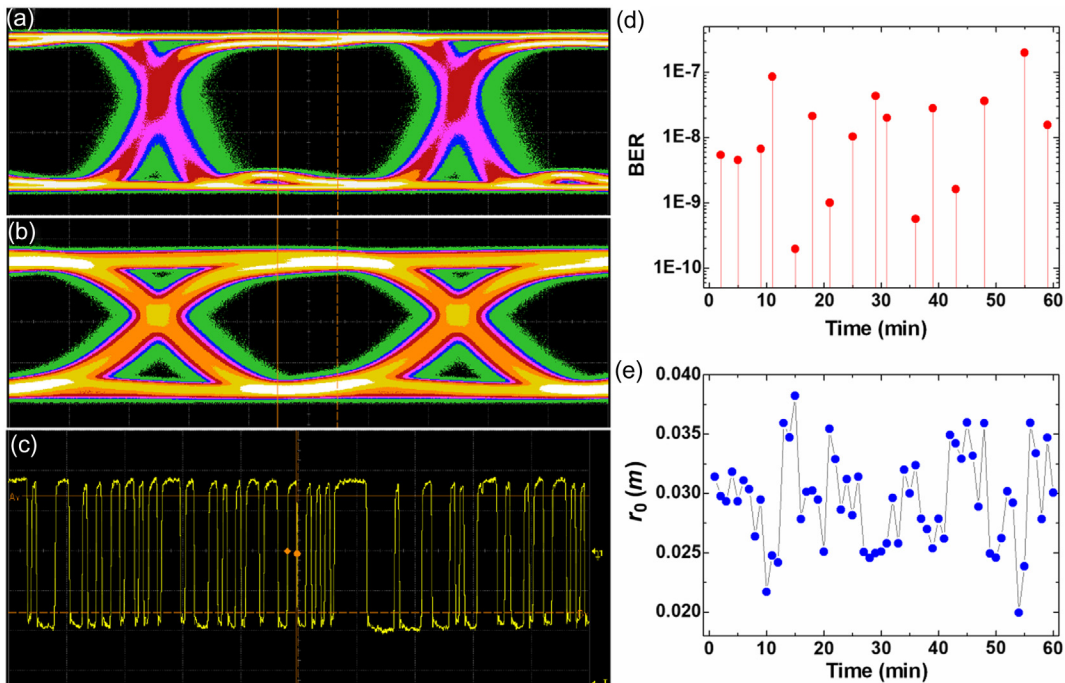


Fig. 12 The oscilloscope screenshots of high-speed eye-diagram acquired by the free-space unequal-arm-length MZI-DPSK receiver: (a) 2.5 Gbps, (b) 5 Gbps, (c) the oscilloscope screenshot of acquired pseudorandom binary signal, (d) BER measurement, and (e) the co-measured Fried coherence parameter r_0 .

experiments were performed within the relatively weak turbulent environment in the night.

3.6 Link Experiments

The 2.5- and 5-Gbps optical communication links have been verified between two buildings in downtown over a distance of 2.4 km. The relatively stable eye-diagrams acquired by the free-space unequal-arm-length MZI-DPSK receiver are shown in Figs. 12(a) and 12(b). The pseudorandom codes with finite-length (1 Mbit), which are differentially encoded, are cyclically transmitted for measuring the BER. Figure 12(c) shows the oscilloscope screenshot of the acquired pseudorandom binary signal. The acquisition time is usually set as 2 to 5 min. Then the BER can be measured by the BER tester or FPGA and is shown in Fig. 12(d). The experiments prove that the obtained BER is better than 10^{-6} . The co-measured r_0 varies from 20 to 37 mm, which is shown in Fig. 12(e).

4 Discussions

Although DPSK modulation can only reduce the temporal phase errors in optical fiber communication,³¹ it is proved that both temporal and spatial phase errors can be eliminated by DPSK modulation and a pupil-matching time-delay self-homodyne interference DPSK optical receiver in a free-space optical communication link. In this work, the pupil-matching time-delayed self-homodyne interference DPSK optical receivers based on the free-space unequal-arm-length MZI and 2×4 90-deg optical hybrid are designed and verified for a space-to-ground optical communication link. To maintain identical wave fronts, the entrance pupil is imaged in both arms onto the same exit pupil. Because the wave fronts within the duration of one bit cannot change because atmospheric turbulence effects are much slower, this ensures that the unequal-arm-length MZI can superimpose identical wave fronts, and optimum modulation contrast is obtained despite a distorted input wave front. Because only free-space optics is used in the time-delay self-homodyne interference DPSK optical receiver, the effects of atmospheric turbulence on the fiber-coupled DPSK system can be neglected where the coupling efficiency of spatial light to single-mode fiber is limited and fluctuates randomly in a satellite-to-ground downlink.³⁵ The maximum system insertion loss is measured to be <1 dB, which can offer support for SNR.

Optical communication links through the atmosphere can be challenging depending on the characteristics of the turbulence for the location, time, and the elevation angle of the transmitted beam. During the optical communication link experiments, the co-measured r_0 varies from 20 to 35 mm. Compared with the published atmospheric value measured by ESA,¹³ the atmospheric conditions can be considered to be worst case. So the free-space unequal-arm-length MZI-DPSK optical receiver can overcome the worst-case atmospheric conditions. This work is a solid foundation for the future satellite-to-ground optical communication link between OGS, which is located at an elevation of 2080 m residing at Urumchi, China, and has better atmospheric conditions, and the coherent laser communication terminal on the Chinese Mozi satellite.

The smaller aperture compared with the Fried coherence parameter has been adopted for the satellite-to-ground BPSK communication links in order to weaken the impairment of atmospheric turbulence because no AO and other

mechanisms can be used at that moment.^{13,14} However, both low receiver power and low receiver power stability will limit the SNR of satellite-to-ground BPSK laser communication links. Moreover, the strong intensity fluctuations cannot be compensated by aperture averaging. Therefore, the small-aperture BPSK receivers were only attempted at excellent astronomical locations (e.g., mountain tops), where the atmospheric conditions are consistent with the link requirements. On the one hand, a time-delay self-homodyne interference DPSK receiver can overcome the atmospheric turbulence. On the other hand, the sensitivity of the time-delay self-homodyne interference DPSK receiver is considerably reduced compared to an ideal homodyne BPSK receiver, which employs a LO to ensure the shot-noise limited performance. The large aperture antenna can receive the most transmitted signal and the SNR can be improved accordingly. A larger aperture receiver in the OGS allows the transmitter power and aperture size of the coherent laser communication terminal on the spacecraft to be reduced significantly. So the $\phi 300$ -mm receiving telescope, which is much larger than the Fried coherence parameter, is used in this work. The $\phi 1.2$ -m larger-aperture receiving telescope and the free-space unequal-arm-length MZI-DPSK optical receiver in the OGS will be applied to the next step satellite-to-ground optical communication downlink.

While the free-space unequal-arm-length MZI-DPSK receiver can effectively eliminate the noise phase caused by atmospheric turbulence, it cannot effectively inhibit the intensity fluctuation caused by beam wander,³² arrival-of-angle fluctuation, and scintillation.³³ The present experimental results confirm that the stability of the eye-diagram for the MZI-DPSK receiver is deteriorated when the turbulence structure profile C_n^2 exceeds $10^{-12} \text{ m}^{-2/3}$ in the worst-case atmospheric conditions. The tracking control loop with tip/tilt correction by an FSM can deal with the problem to some extent. Now the high-dynamic range optical automatic gain controller is in development. The multiaperture DPSK receivers with inherent superposition are also under research.

In this work, the data rate of 2.5 Gbps is equivalent to an OPD of 120 mm in air, and the data rate of 5 Gbps is equivalent to an OPD of 60 mm in air. Compared with the traditional BPSK optical communication link, the maximum transmission bit rate of time-delay self-homodyne interference DPSK receiver is limited by the geometry of free-space unequal-arm-length interferometer. The higher data-rate DPSK receiver with an integrated Michelson interferometer structure is under development. Due the high-speed relative motion between the satellite and the ground terminal, the terminals on the OGS receive a high Doppler frequency shift over the satellite-ground channel. The amount of Doppler shift is estimated to be more than gigahertz, which depends on the altitude of orbit of the LEO/GEO-ground downlink. In future work, the influence of the Doppler shift on high data-rate optical communication link will also be investigated carefully.

5 Conclusions

In conclusion, a pupil-matching time-delay self-homodyne interference DPSK receiver based on a free-space unequal-arm-length MZI and 2×4 90-deg optical hybrid for a high data-rate space-to-ground optical communication link is

presented. The free-space unequal-arm-length MZI splits the signal into two paths and recombines them. The delayed OPD is equivalent to the duration of one bit. This method, based on the free-space difference of two successive wave fronts, requires neither AO nor OPLL. In addition to detailed theoretical analysis, the relatively stable 2.5- and 5-Gbps optical communication link has already been performed with a ϕ 300-mm receiving telescope between two buildings in downtown over a distance of 2.4 km. The measured BER is better than 10^{-6} in the worst-case atmospheric conditions, which is monitored by atmospheric measurement. Both theoretical and experimental results can manifest that the time-delay self-homodyne interference DPSK receiver can overcome the distorted wave front and eliminate the noise phase caused by the atmospheric turbulence. The time-delay self-homodyne interference DPSK receiver has great significance for the future developments of satellite-to-ground optical communication link.

Acknowledgments

This work was supported by the Chinese Academy of Sciences, National Natural Science Foundation of China (Grant Nos. 60908029 and 61275110). With this paper, I would like to pay great tribute to Prof. Liren Liu.

References

- V. W. S. Chan, "Free-space optical communications," *J. Lightwave Technol.* **24**(12), 4750–4762 (2006).
- T. Nielsen and G. Oppenhaeuser, "In orbit test result of an operational inter-satellite link between ARTEMIS and SPOT4, SILEX," *Proc. SPIE* **4635**, 1–15 (2002).
- M. Reyes et al., "Preliminary results of the in-orbit test of ARTEMIS with the optical ground station," *Proc. SPIE* **4635**, 38–49 (2002).
- M. Toyoshima et al., "Ground-to-satellite optical link tests between the Japanese laser communication terminal and the European geostationary satellite ARTEMIS," *Proc. SPIE* **5338**, 1–15 (2004).
- M. Toyoshima et al., "Long-term statistics of laser beam propagation in an optical ground-to-geostationary satellite communications link," *Proc. IEEE* **53**(2), 842–850 (2005).
- M. R. Garcia-Talavera et al., "Ground to space optical communication characterization," *Proc. SPIE* **5892**, 589202 (2005).
- T. Jono et al., "Overview of the inter-orbit and the orbit to ground laser communication demonstration by OICETS," *Proc. SPIE* **6457**, 645702 (2007).
- X. Sun et al., "Free space laser communication experiments from Earth to the lunar reconnaissance orbiter in lunar orbit," *Opt. Express* **21**(2), 1865–1871 (2013).
- D. M. Cornwell, "NASA's optical communications program for 2015 and beyond," *Proc. SPIE* **9354**, 93540E (2015).
- L. G. Kazovsky, G. Kalogerakis, and W. T. Shaw, "Homodyne phase-shift-keying systems: past challenges and future opportunities," *J. Lightwave Technol.* **24**, 4876–4884 (2006).
- B. Smutny et al., "In-orbit verification of optical inter-satellite communication links based on homodyne BPSK," *Proc. SPIE* **6877**, 687702 (2008).
- B. Smutny et al., "5.6 Gbps optical inter-satellite communication link," *Proc. SPIE* **7199**, 719906 (2009).
- R. A. Fields et al., "5.625 Gbps bidirectional laser communications measurements between the NFire satellite and an optical ground station," *Proc. SPIE* **8184**, 81840D (2011).
- S. Seel et al., "Space to ground bidirectional optical communication link at 5.6 Gbps and EDRS connectivity outlook," in *Proc. IEEE Aerosp. Conf.*, pp. 1–7 (2011).
- J. C. Ricklin et al., "Atmospheric channel effects on free-space laser communication," *J. Opt. Fiber Commun. Rep.* **3**, 111–158 (2006).
- D. L. Fried and J. D. Cloud, "Propagation of an infinite plane wave in a randomly inhomogeneous medium," *J. Opt. Soc. Am.* **56**, 1667–1676 (1966).
- Z. Sodnik et al., "Adaptive optics and ESA's optical ground station," *Proc. SPIE* **7464**, 746406 (2009).
- T. Berkefeld et al., "Adaptive optics for space-to-ground laser communication at the 1m telescope of the ESA optical ground station, Tenerife, Spain," *Proc. SPIE* **7736**, 77364C (2010).
- C. Liu et al., "Performance evaluation of adaptive optics for atmospheric coherent laser communications," *Opt. Express* **22**, 15554–15563 (2014).
- W. Liu et al., "Performance evaluation of coherent free space optical communications with a double-stage fast-steering-mirror adaptive optics system depending on the Greenwood frequency," *Opt. Express* **24**, 13288–13302 (2016).
- C. Liu et al., "Adaptive optics for the free-space coherent optical communications," *Opt. Commun.* **361**, 21–24 (2016).
- J. B. Stewart et al., "Comparing adaptive optics approaches for NASA LCRD ground station #2," *Proc. SPIE* **8610**, 86100M (2013).
- S. M. Zhao et al., "Aberration corrections for free-space optical communications in atmosphere turbulence using orbital angular momentum states," *Opt. Express* **20**(1), 452–461 (2012).
- I. B. Djordjevic and M. Arabaci, "LDPC-coded orbital angular momentum (OAM) modulation for free-space optical communication," *Opt. Express* **18**(24), 24722–24728 (2010).
- M. Malik et al., "Influence of atmospheric turbulence on optical communications using orbital angular momentum for encoding," *Opt. Express* **20**(12), 13195–13200 (2012).
- X. L. Yin et al., "Adaptive turbulence compensation with a hybrid input-output algorithm in orbital angular momentum-based free-space optical communication," *Appl. Opt.* **57**(26), 7644–7650 (2018).
- Z. Sodnik and M. Sans, "Extending EDRS to laser communication from space to ground," in *Proc. Int. Conf. Space Opt. Syst. and Appl. (ICSOS)*, pp. 13–2 (2012).
- G. D. Xie, A. H. Dang, and H. Guo, "Effects of atmosphere dominated phase fluctuation and intensity scintillation to DPSK System," in *Proc. IEEE Int. Conf. Commun.*, pp. 1–6 (2011).
- Y. N. Zhi et al., "High data-rate differential phase shift keying receiver for satellite-to-ground optical communication link," *Proc. SPIE* **8517**, 85170F (2012).
- R. Garreis and C. Zeiss, "90-deg optical hybrid for coherent receivers," *Proc. SPIE* **1522**, 210–219 (1991).
- A. Gnauck and P. J. Winzer, "Optical phase-shift-keyed transmission," *J. Lightwave Technol.* **23**(1), 115–130 (2005).
- J. Ma et al., "Influence of beam wander on bit-error rate in a ground-to-satellite laser uplink communication system," *Opt. Lett.* **33**, 2611–2613 (2008).
- M. Reyes et al., "Propagation statistics of ground-satellite optical links with different turbulence conditions," *Proc. SPIE* **5572**, 211–222 (2004).
- X. P. Ma et al., "Performance analysis of pupil-matching optical differential receivers in space-to-ground laser communication," *Appl. Opt.* **53**(14), 3010–3018 (2014).
- Q. B. Yang et al., "Effects of atmospheric turbulence on fiber-coupled DPSK system in satellite-to-ground downlink," *Results Phys.* **11**, 938–943 (2018).

Yanan Zhi received his PhD in optical engineering from Shanghai Institute of Optics and Fine Mechanics, Chinese Academy of Sciences, Shanghai, China, in 2007. He is an associate professor in the Laboratory of 3-D Optics and Depth Sensing Technology, Zhejiang University of Science and Technology, Zhejiang, China. From 2007 to 2014, he worked as an associate researcher at Shanghai Institute of Optics and Fine Mechanics. From 2014 to 2016, he worked as a research assistant professor in the Department of Bioengineering, University of Illinois at Chicago, USA. He is the author of more than 30 journal papers. His current research interests include synthetic aperture imaging lidar and free-space optical communication.

Liren Liu is a distinguished professor at Shanghai Institute of Optics and Fine Mechanics, Chinese Academy of Sciences. He is a renowned scientist in the areas including crystal optics, holographic optics, optical computing, optical storage, laser communication, and synthetic aperture lidar. He is a prolific author and has published more than 700 journal papers to his credit. He is also a tireless advocate for young scientists having served as a mentor and advisor.

Biographies of the other authors are not available.